文章编号：0253-2409(2015)10-1258-09

Effect of preparation methods on the performance of MnO_x-TiO_2 adsorbents for Hg^0 removal and SO_2 resistance

ZHANG An-chao[1,*], ZHANG Zhi-hui[1],
SHI Jin-ming[2], CHEN Guo-yan[1], ZHOU Chang-song[3], SUN Lu-shi[3]
(1. *School of Mechanical and Power Engineering, Henan Polytechnic University, Jiaozuo* 454003, *China*;
2. *Institute of Energy Conversion, Jiangxi Academy of Sciences, Nanchang* 330096, *China*;
3. *State Key Laboratory of Coal Combustion, Huazhong University of Science and Technology, Wuhan* 430074, *China*)

Abstract: Aiming at the difficulty of elemental mercury (Hg^0) removal from flue gas due to its indissolubility in water and the problem of lower SO_2 resistance performance of manganese-based adsorbent, the MnO_x-TiO_2 adsorbents prepared with impregnation (IM), sol-gel (SG) and deposition-precipitation method (DP) were employed to remove Hg^0 in the absence and presence of SO_2. The adsorbents were characterized by N_2 adsorption-desorption, TG-DSC, XRD, TEM, H_2-TPR, and XPS techniques. The results showed that Hg^0 removal performance over MnO_x-TiO_2 adsorbents was markedly influenced by the preparation methods. The adsorbent prepared by DP method exhibited a superior activity for Hg^0 adsorption and the best SO_2 resistance performance. The characterization results indicated that the Hg^0 removal activity did not correlate with the BET surface area. The preparation method of deposition-precipitation could not only lead to an increase of reducibility and high dispersion of MnO_x, but also significantly enhance a migration of well-dispersed active phase from bulk to surface, resulting in a higher Mn^{4+}/Mn ratio and the presence of abundant chemisorbed oxygen, which would play an important role in promoting Hg^0 removal.

Keywords: preparation method; MnO_x-TiO_2; Hg^0 removal; SO_2 resistance
CLC number: X511 **Document code**: A

Mercury pollution has received considerable attention from environmental researchers due to its high volatility, long persistence and strong bioaccumulative properties[1]. Coal-fired utility boilers and municipal waste incineration plants are major anthropogenic sources of mercury emissions[2,3]. In China, about 38% of mercury emission comes from coal combustion[4,5]. Mercury in coal is released in three forms: elemental (Hg^0), oxidized (Hg^{2+}) and particle-bound (Hg^p)[5]. Most of existing air pollution control technologies, such as electrostatic precipitators and baghouses, can effectively remove the Hg^p. The oxidized form mercury, which is generally soluble in water, can be efficiently captured by a wet scrubber[6,7]. However, Hg^0 is very difficult to be controlled from flue gas because of its high volatility and indissolubility in water[7,8].

In recent years, numerous efforts have been focused on the removal of Hg^0 from flue gas since the present severe environmental policy. Among them, metal oxides have been considered as a novel alternative to traditional mercury adsorbents because of its lower cost and higher activity. In particular, manganese oxide (MnO_x) is one of the potential adsorbents/catalysts to remove NO_x[9~15], Hg^0[16~21] and other pollutants[22] at lower temperature. Qiao et al[16] reported that MnO_x/Al_2O_3 had significant oxidation activity on Hg^0 removal in the presence of HCl. Ji et al[17] found that using CO as reductant, MnO_x/TiO_2 was shown to be much effective for both Hg^0 removal and low-temperature NO-SCR. It is clear that the promoter of MnO_x can greatly enhance the Hg^0 removal activity, however, the promotional level between promoter and support may be strongly dependent on the preparation conditions, for example, the preparation method. Not unexpectedly, many methods have been employed to prepare Mn-based adsorbents/catalysts. For example, the comparison of MnO_x-TiO_2 catalysts prepared by conventional wet-impregnation (IM) method and deposition-precipitation (DP) method was studied by Wu et al[15]. The results exhibited that the maximum NO conversion over MnO_x(0.3)/TiO_2(DP) could reach 89% at 250 ℃, which was much higher than that over the catalyst prepared by IM method (40% at

Received: 2015-07-01; **Revised**: 2015-08-23.

* **Corresponding author**: Tel: 15039126550, E-mail: anchaozhang@126.com.

The project was supported by the National Natural Science Foundation of China (51306046, 51166004, 51376073), the Fundamental Research Funds for the Universities of Henan Province (NSFRF140204).
国家自然科学基金(51306046, 51166004, 51376073)和河南省高校基本科研业务费(NSFRF140204)
本文的英文电子版由 Elsevier 出版社在 ScienceDirect 上出版(http://www.sciencedirect.com/science/journal/18725813).

250 ℃). MnO_x-CeO_2 catalysts synthesized by Qi et al[23] using citric acid method (CA), impregnation method (IM) and coprecipitation method (CP). They found that the maximum NO conversion decreased in the sequence of MnO_x-CeO_2 (CA) > MnO_x-CeO_2 (CP) > MnO_x-CeO_2 (IM). Obviously, the method used to prepare Mn-based adsorbents/catalysts is one of the key factors in determining the performance through changing their physicochemical properties, such as surface area, particle size, particle distribution and dispersion of the active components. The effects of flue gas compositions, such as O_2, SO_2, NO and HCl, on MnO_x-based adsorbents/catalysts have been extensively studied in previous literatures[19,21]. As reported[16,17], the adsorbent/catalysts prepared by impregnation method have been extensively researched in the field of Hg^0 removal from flue gas. However, the preparation methods such as deposition-precipitation with higher NO-SCR conversion efficiency are frequently not adopted. Due to the presence of surface acidity, TiO_2 containing support materials were reported to suppress the SO_2 poisoning[24] and widely employed as support[9,12,13,15,17,20~22]. To the best of our knowledge, however, little work has been done on the effect of preparation methods of MnO_x-TiO_2 adsorbents for Hg^0 removal and SO_2 resistance. Thus, an in detail investigation of different preparation methods on MnO_x-based adsorbent is of necessary, which could be important for further practical use.

In this work, three MnO_x-TiO_2 adsorbents were prepared using impregnation, sol-gel and deposition-precipitation methods, respectively. The influences of preparation methods on Hg^0 removal and SO_2 resistance over MnO_x-TiO_2 adsorbents were investigated. All samples were characterized by N_2 adsorption-desorption, TG-DSC, XRD, TEM, H_2-TPR and XPS techniques. The characterization results were related with the activities of MnO_x-TiO_2 adsorbents for Hg^0 removal.

1 Experimental

1.1 Adsorbents preparation

1.1.1 Impregnation method

10 g of P25 TiO_2 (Degussa, German) support was added to a beaker containing 50 mL of purified water under vigorous stirring for 1 h. A certain amount of manganese nitrate was quickly poured into the above mixture with continuous stirring for another 2 h. The mixture was then stored for about 10 h at room temperature and dried at 105 ℃ for 24 h. Finally, the material was ground into power and calcined at 450 ℃ for 5 h in air condition, which was designated as MnTi-IM.

1.1.2 Sol-gel method

First, anhydrous ethanol (0.2 mol), acetic acid (0.18 mol) and deionized water (0.55 mol) were uniformly mixed at room temperature (denoted as solution A). Second, aqueous solutions of manganese nitrate, anhydrous ethanol (0.5 mol) and tetrabutyl titanate (0.1 mol) were blended under rapid stirring (denoted as solution B). Then, solution A was slowly added into solution B with vigorous stirring until the sol was yielded. After aging for several days, the sol transformed to gel. The gel was crushed and dried at 105 ℃ for 48 h. Finally, the material was ground into power and calcined at 450 ℃ for 5 h in air, which was named as MnTi-SG.

1.1.3 Deposition-precipitation method

A certain amount of manganese nitrate was quickly added to a slurry solution (80 mL) containing 10 g of P25 TiO_2 with vigorous stirring. Then, a mixed solution of $NH_3 \cdot H_2O$ (15%) and NH_4HCO_3 (15%) was added dropwise to the above mixture until a constant pH value of 10 was obtained. The mother mixture solution was aged at 60 ℃ for 2 h. The resulting precipitate was filtered and washed several times with deionized water. Finally, the filtered sample was dried at 105 ℃ for 24 h and then calcined at 450 ℃ for 5 h in air, which was denoted as MnTi-DP.

All the chemical reagents were of analytical grade without further purification. The molar ratio of Mn to Ti was 1∶10. All prepared catalysts were pressed, crushed and sieved to 60 ~ 80 mesh prior to Hg^0 removal evaluation.

1.2 Activity tests

The Hg^0 removal tests were carried out in a fixed-bed quartz tube reactor (i. d. 10 mm) under atmospheric pressure. The detailed description of the experimental setup and procedure were given elsewhere[21]. To explore the effect of preparation methods on Hg^0 removal and SO_2 resistance, baseline (BL) flue gas, which only contained 6% O_2, 12% CO_2, balanced N_2, and 560 mg/m^3 of SO_2 (when used) were considered. The feed gases at a total flow rate of 1 L/min were metered using calibrated electronic mass flow controllers. The inlet Hg^0 concentration (C_{in}) was about 75 μg/m^3, and about 0.05 g sample mixed with 2.0 g inert SiO_2 (with the same size like adsorbent) was used if there was no special specification. To avoid physical adsorption, the employed SiO_2 had been calcined at 800 ℃. The vapor-phase Hg^0 concentrations of influent and

effluent were determined continuously using a SG-921 cold vapor atomic absorption spectroscopy (CVAAS) mercury analyzer (Jiangfen Ltd. China). The Hg^0 removal efficiency and adsorption capacity within 10 h over MnO_x-TiO_2 were used as follows:

$$\eta = (1 - \frac{C_{out}}{C_{in}}) \times 100 \quad (1)$$

$$Q = \frac{C_{in}}{m} \int_0^{t_1} \eta \times V \times dt \quad (2)$$

where η is the Hg^0 removal efficiency (%) at a certain time, C_{in} and C_{out} represent the Hg^0 concentrations corresponding to the inlet and outlet ($\mu g/m^3$), Q is the cumulative Hg^0 adsorption capacity per gram of adsorbent ($\mu g/g$), m is the mass of tested adsorbent (g), V denotes the total flow rate of feed gas (m^3/min) and t_1 represents the final time of breakthrough curve (min), respectively. The experimental error was inevitable. Hence, the cumulative Hg^0 adsorption capacities were carried out in triplicates to obtain parallel results and reduce uncertainties.

1.3 Characterization

The specific surface area and pore parameter of the sample were determined by N_2 physisorption method at liquid-nitrogen temperature (77 K) on a Tristar Ⅱ 3020 surface area and porosimeter (Micromeritics Instrument Corporation, USA). The specific surface area of the sample was measured by using Brunauer-Emmett-Teller (BET) method. The pore volume and pore size distribution were calculated by Barrett-Joiner-Halenda (BJH) method.

Thermal gravimetric and differential scanning calorimetry (TG-DSC) analyses of the adsorbents were performed on a SDT Q600 thermogravimetric analyzer (TA Instrument Corporation, USA). Constant mass of a sample was used in order to avoid the effect of variation in sample weight on peak shape and temperature. The temperature was raised from room temperature to 800 ℃ with a linear heating rate of 10 ℃/min.

X-ray diffraction (XRD) experiments were carried out on a Bruker D8 Advance X-ray diffractometer (Bruker Corporation, Germany) employing Cu $K\alpha$ radiation as X-ray source. The scanning range (2θ) was from 10° to 80° with a step size of 0.02°. The accelerating voltage and applied current were 40 kV and 40 mA, respectively.

Transmission electron microscopy (TEM) images were taken on a FEI Tecnai G20 high-resolution transmission electron microscope (FEI Company, USA) with an acceleration voltage of 200 kV.

Hydrogen gas temperature-programmed reduction (H_2-TPR) measurements were conducted on an AutoChem Ⅱ 2920 chemisorption instrument (Micromeritics Instrument Corporation, USA). The sample (about 100 mg) was first pretreated at 200 ℃ for 1 h and cooled to 50 ℃ in Ar flow. The treated sample was reduced from 50 to 800 ℃ at a linear heating rate of 10 ℃/min in 15% H_2/Ar with a flow rate of 30 mL/min. The H_2 consumption was recorded continuously with a TCD detector.

Raman spectra were performed on a LabRAM HR800 Raman microspectrometer (Horiba Jobin Yvon Corporation, France) with YAG solid state laser (532 nm).

X-ray photoelectron spectroscopy (XPS) signals were carried out on a Thermo ESCALAB 250XI spectrometer (Thermo Fisher Scientific, USA) with an Al $K\alpha$ radiation ($h\nu$ = 1 486.6 eV). The C 1*s* line at 284.6 eV was used as a reference for the binding energy (BE) calibration. The spectra were fitted by XPS Peak 4.1 program.

2 Results and discussion

2.1 Hg^0 adsorption activity over different adsorbents

Figure 1 shows the Hg^0 adsorption capacities over MnO_x-TiO_2 adsorbents with different preparation methods under baseline (BL) condition. As reported, Hg^0 removal by metal oxide (MO_x) adsorbent can be successfully interpreted by the Mars-Maessen mechanism[3], where Hg^0 bonds with lattice oxygen and/or chemisorbed oxygen of the adsorbent to form weakly bonded $Hg-O-M-O_{x-1}$ species and then formed HgO. The consumption of lattice oxygen and/or chemisorbed oxygen can be replenished by gas phase O_2. From Figure 1, it can be observed that the three adsorbents all showed high Hg^0 adsorption capacities, especially the adsorbent prepared by the deposition-precipitation method. For a running time of 10 h, the cumulative Hg^0 adsorption capacity of MnTi-DP reaches as high as 615 $\mu g/g$, which is approximately 1.4 times of MnTi-IM. The Hg^0 adsorption performance is in the sequence of MnTi-DP > MnTi-SG > MnTi-IM, indicating that the preparation method plays a significant role in Hg^0 removal.

2.2 SO_2 resistance on Hg^0 removal

The effect of SO_2 on Hg^0 removal efficiencies over MnO_x-TiO_2 adsorbents prepared by different methods is displayed in Figure 2. In order to intuitively investigate the effect of SO_2 on Hg^0 removal efficiency, the Hg^0 removal experiments are first performed in the absence of SO_2 for about 20 min

and then 560 mg/m^3 of SO_2 is injected. It is worth noting that the addition of SO_2 results in a small and temporary enhancement of Hg^0 removal for all samples during the initial 10 min, which could be owed to the formation of $HgSO_4$ according to the following reactions:

$$SO_2 + O^* \rightarrow SO_3 \quad (3)$$

$$Hg^0 + O^* \rightarrow HgO \quad (4)$$

$$HgO + SO_3 \rightarrow HgSO_4 \quad (5)$$

$$Hg^0 + SO_3 + O^* \rightarrow HgSO_4 \quad (6)$$

where O^* represents the active site on the MnO_x-TiO_2 surface.

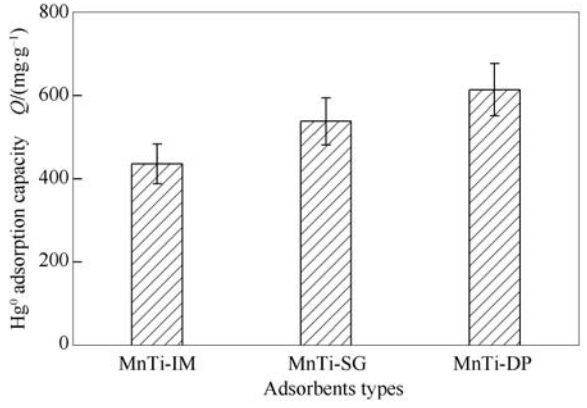

Figure 1　Hg^0 adsorption capacities over different adsorbents

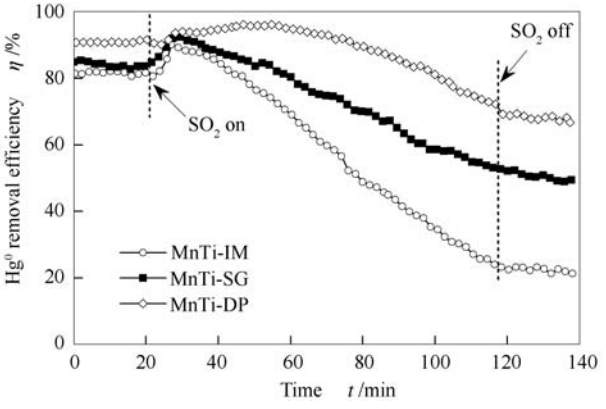

Figure 2　Effect of SO_2 on Hg^0 removal efficiencies over different adsorbents

With increasing reaction time, Hg^0 removal efficiencies of all samples decrease because Mn-based adsorbents are sensitive to SO_2 poisoning[25]. Especially, Hg^0 removal efficiency of MnTi-IM decreases significantly to less than 30 % in 100 min. According to the literatures[16~21], MnO_2 itself is an active reaction site for effective Hg^0 removal. However, once MnO_2 is poisoned by SO_2 to produce $MnSO_4$, the sulfate species would deposit on the surface of adsorbent and the consumptions of active MnO_x and chemisorbed oxygen by SO_2 show an irreversibly negative effect on Hg^0 removal due to higher thermostability of $MnSO_4$[25]. Thus, the proposed Mars-Maessen mechanism can hardly come true. When SO_2 is cut off from the reaction, the activity of all adsorbents could not be able to restore their initial activities. Nevertheless, by comparison, it could be concluded that MnTi-DP has the best SO_2 resistance performance, which may be due to its high dispersion of MnO_x onto TiO_2 and good redox ability.

2.3　Adsorbents characterization

2.3.1　N_2 adsorption-desorption analysis

The textural properties of MnO_x-TiO_2 adsorbents with three preparation methods are summarized in Table 1. It can be observed that the BET surface area and total pore volume of P25 TiO_2 are 49.63 m^2/g and 0.260 cm^3/g, respectively. Compared with P25 TiO_2, the BET surface areas and total pore volumes of MnTi-IM and MnTi-DP are slightly decreased, confirming the successful formation of MnO_x onto the surface of TiO_2. Among the three adsorbents, MnTi-SG shows the highest BET surface area (81.47 m^2/g), illustrating that the sol-gel method could bring out an increase in porosity compared with impregnation and deposition-precipitation methods. This also suggests that the difference in preparation methods could result in different pore property. In addition, although the BET surface area of MnTi-DP is lower than that of MnTi-SG, it exhibits higher Hg^0 removal capacity. Hence, the Hg^0 removal activity does not correlate with the BET surface area. This implied that the physical characteristics are not the main contributor for Hg^0 removal.

Table 1　Physical properties of the adsorbents

Sample	BET surface area A/(m^2·g^{-1})	Total pore volume v/(cm^3·g^{-1})	Mean pore diameter d/nm
P25 TiO_2	49.63	0.260	20.56
MnTi-IM	43.13	0.208	19.29
MnTi-SG	81.47	0.220	10.75
MnTi-DP	48.76	0.214	17.67

2.3.2　TG-DSC analysis

To get more information about MnO_x species variation and weight loss as a result of the calcination temperature increasing, TG-DSC measurements of the three uncalcined MnO_x-TiO_2 samples are performed and presented in Figure 3. In order to clearly

understand their TG changes, the enlarged curves are also given in insert map. From the TG curves, it can be seen that all adsorbents show four continuous weight losses during the entire heating process. The total weight loss of MnTi-SG could reach as high as 30%, whereas the weight losses of MnTi-IM and MnTi-DP were only about 4% and 5%, respectively. The initial weight loss from room temperature to 150 ℃ accompanied by endothermic peaks in DSC should be assigned to desorption of physically adsorbed water[9]. For MnTi-IM, the broad peak emerged in DSC curve from 200 to 600 ℃ is attributed to the decomposition of nitrate precursor and phase variation of MnO_x species. The DSC curve of MnTi-DP shows three peaks at 200, 252 and 445 ℃, respectively, which could be related to the decomposition of the manganese hydroxide[26]. As for MnTi-SG, the remarkable mass loss in the range of 200 ~ 450 ℃ should be assigned to the decomposition of organic solvent, unbound stabilizing acid and phase transformation of MnO_x. Jiang et al[13] had already pointed out the evidence for the appearance of this phenomenon. The last mass losses emerging after 650 ℃ are owed to the phase transformation of anatase TiO_2, and MnO_x[27]. Therefore, the results indicate that the calcination temperature of 450 ℃ could guarantee the decomposition of precursors and the formation of active MnO_x.

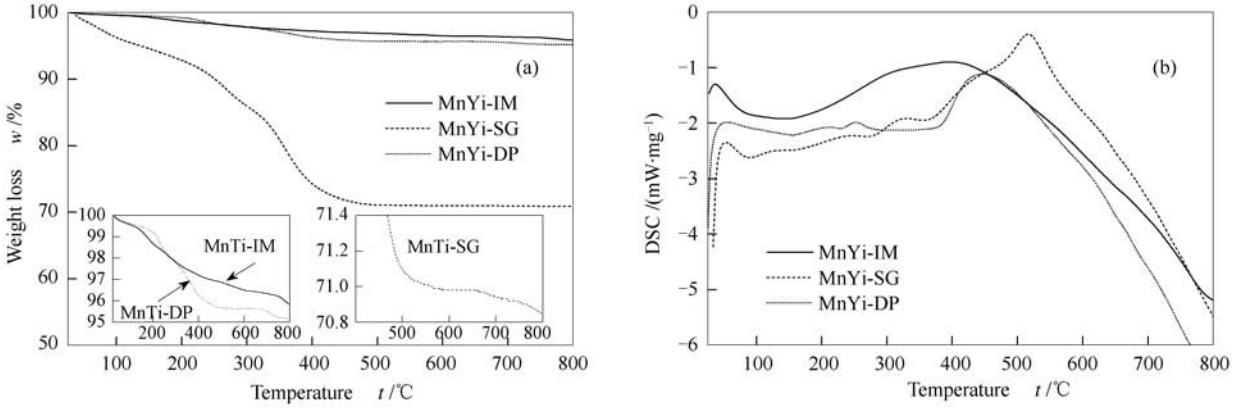

Figure 3 TG (a) and DSC (b) curves for uncalcined MnTi-IM, MnTi-SG, and MnTi-DP

2.3.3 XRD and TEM results

The XRD patterns of MnO_x-TiO_2 samples are shown in Figure 4. In our previous study[21], it was found that the commercial P25 TiO_2 contained a small content of rutile and anatase in large amount. Accordingly, MnTi-IM and MnTi-DP display very similar XRD patterns like P25 TiO_2. The addition of MnO_x does not lead to significant changes in the positions and intensities of typical TiO_2 diffractions, whereas some small XRD peaks at 2θ = 28.7°, 56.7° and 64.4° (JCPDS 24-0735) corresponding to MnO_2 was slightly detected in MnTi-IM due to good dispersion and small crystallite size of MnO_x. Compared with MnTi-IM and MnTi-DP, no clear peak associated with MnO_x appears in MnTi-SG sample. Moreover, the peaks assigned to anatase TiO_2 become weaker and broader, implying that MnO_x is well dispersed and/or kept as amorphous phase. The similar phenomena were also observed by Jiang et al[13].

To obtain the specific distribution of particles and MnO_x species, the real morphologies of samples were further explored by TEM technique. As presented in Figure 5 (a), (c) and (e), the three prepared adsorbents are nano-scaled. However, they are different significantly in size. The MnTi-SG particles are much smaller than those of MnTi-IM and MnTi-DP. By contrast, the dispersion of MnTi-SG is very poor. In HRTEM images (Figure 5 (b), (d) and (f)), well-crystallized anatase TiO_2 (the lattice fringe of (101) plane is 0.35 nm) and MnO_2 (the lattice fringe of (010) plane is 0.29 nm) can be seen in MnTi-IM and MnTi-SG samples, whereas only crystalline structure of TiO_2 is detected in MnTi-DP, implying higher dispersion of MnO_x species, which is in accordance with previous report[9].

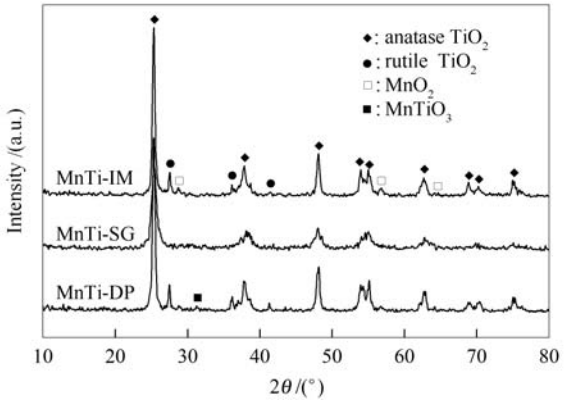

Figure 4 XRD patterns of MnTi-IM, MnTi-SG and MnTi-DP

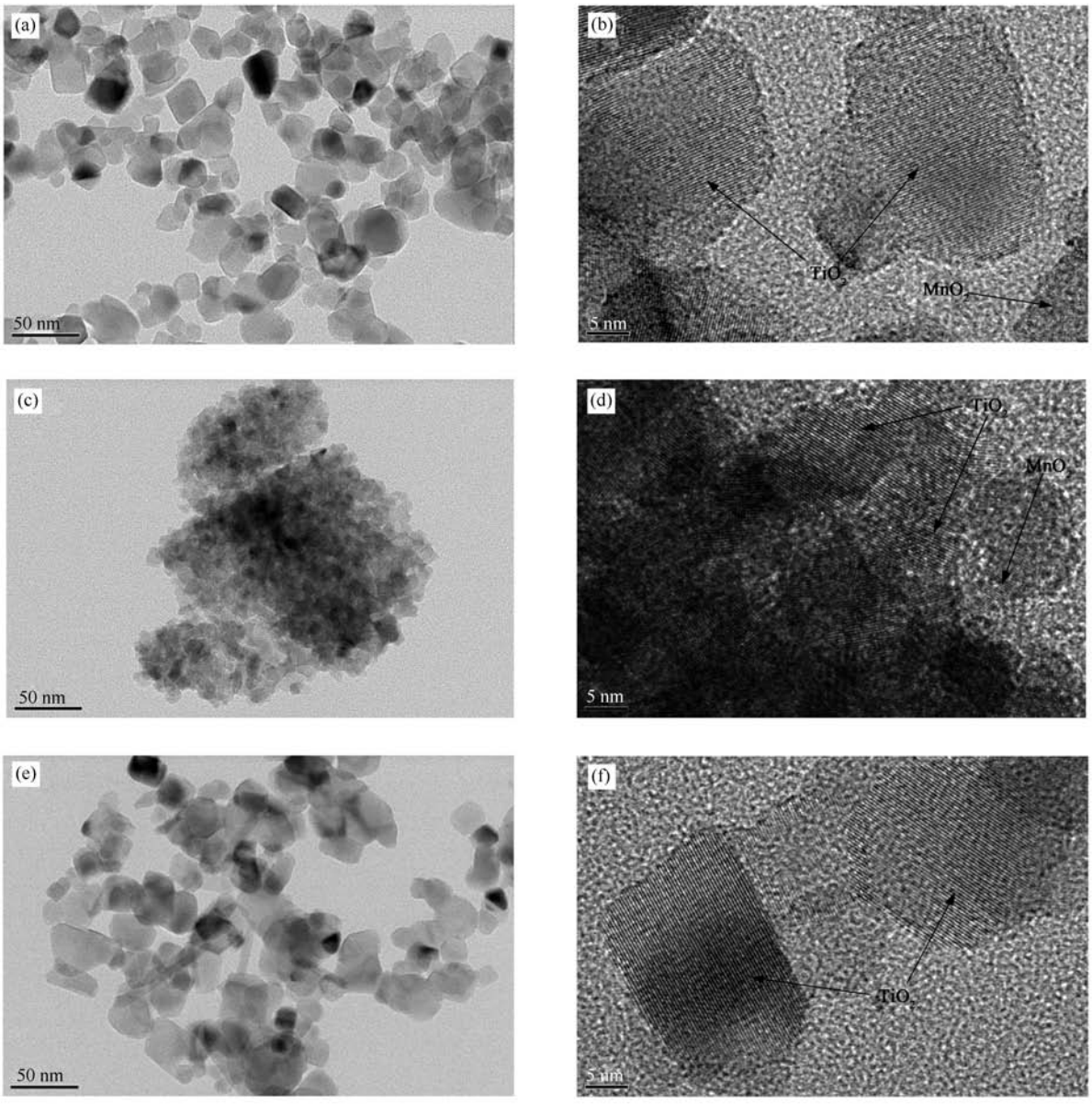

Figure 5　TEM images of samples with low (left) and high (right) magnification
(a), (b): MnTi-IM; (c), (d): MnTi-SG; (e), (f): MnTi-DP

2.3.4　H_2-TPR and Raman results

Figure 6 presents the H_2-TPR profiles of MnO_x-TiO_2 samples with different preparation methods. The H_2-TPR curves of MnTi-IM and MnTi-DP show two distinct reduction peaks within the temperature range of 200 ~ 500 ℃, which may be assigned to the reduction of $MnO_2 \rightarrow Mn_2O_3 \rightarrow MnO$[10,28], while MnTi-SG exhibit three successive reduction peaks. It had been reported that the reduction of Mn^{2+} in MnO_x was completed up to 550 ℃ and further reduction to metallic Mn did not proceed until 1 200 ℃[29]. Thus, the last one in MnTi-SG located at 572 ℃ could correspond to the reduction of Mn^{2+} state from analogous pyrophanite formed due to the presence of Ti^{4+} species[10]. This implies that there was strong interaction among Mn, Ti and oxygen in MnTi-SG, which makes it difficult to be reduced by gaseous H_2 at lower temperature. In addition, among these adsorbents, MnTi-SG exhibits the lowest reduction intensity in the H_2-TPR profiles, which is probably due to the type and strength of the interaction between supported MnO_x species and the titania support. Similar phenomenon was also found by Gao et al[30] when CeO_2/TiO_2 catalysts were prepared by different methods. Moreover, it is clear that MnTi-DP shows lower reducing temperature, illustrating an increase of reducibility. It had been reported that more reducible species was favorable for increasing the catalytic activity[31].

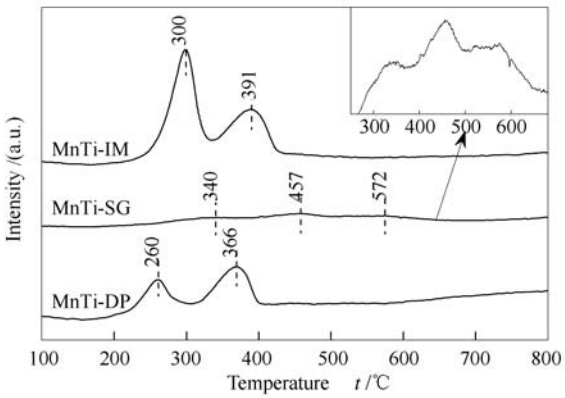

Figure 6 H_2-TPR profiles of MnTi-IM, MnTi-SG and MnTi-DP

The nature of MnO_x species on TiO_2 supports is further confirmed by Raman spectroscopy as shown in Figure 7. The spectra of all samples show five peaks centered at 152, 202, 400, 510 and 628 cm^{-1}, which are attributed to typical anatase TiO_2[22], consistent with the results of XRD analysis. Regarding the fact of the Raman peaks of MnO_2 are overlapped with strong band of TiO_2 in the regions, one small peak at 478 cm^{-1} assigning to β-MnO_2 phase appears[12] in MnTi-SG and MnTi-DP, and no additional characteristic vibration band of Mn–O is observed. By contrast, it is worthy to note that the intensities of anatase bands in MnTi-SG are more intensive. In addition, the Raman intensity of MnTi-DP is lower than that of MnTi-IM, verifying that the presence of MnO_x onto TiO_2 is of amorphous structure. The amorphous structure is usually of higher active than the crystallized one.

2.3.5 XPS analysis

To obtain better insight into the nature of the active species and the surface atomic compositions of the adsorbents, the three adsorbents are examined using XPS technique as shown in Figure 8. The surface compositions and surface atomic ratios of the samples calculated by XPS results are summarized in Table 2. Figure 8(a) shows the XPS spectrum of Ti 2*p*. Two well-defined characteristic peaks assigning to Ti $2p_{1/2}$ at 464.2 eV and Ti $2p_{3/2}$ at 458.4 eV appear for all samples, showing Ti mainly being in the form of Ti^{4+} oxidation state[17,32]. It is clear that compared with MnTi-IM and MnTi-SG, the intensity of Ti $2p_{3/2}$ peak of MnTi-DP significantly increases, which is possibly owing to an improvement in the electron affinity of Ti.

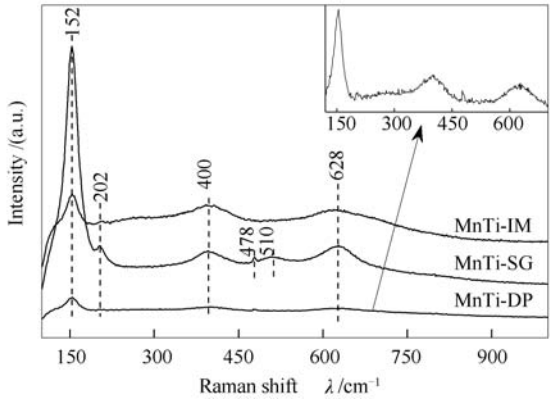

Figure 7 Raman spectra of the samples

The XPS results for Mn 2*p* are shown in Figure 8(b). The Mn 2*p* region is composed of a doublet peak with Mn $2p_{1/2}$ located at 653.3 eV and Mn $2p_{3/2}$ centered at 641.2 eV, revealing the characteristic of multiple valence manganese oxides. According to the literatures[33,34], the Mn $2p_{3/2}$ binding Energy of Mn^{2+}, Mn^{3+} and Mn^{4+} in the three adsorbents could be separated in the ranges of 640.3 ~ 640.7, 641.6 ~ 642.3 and 643.2 ~ 644.5 eV, respectively. It is obvious that the intensity of Mn 2*p* in MnTi-DP is bigger than the other two adsorbents, indicating the higher content of Mn as shown in Table 2. Also, for MnTi-SG and MnTi-DP, the surface atomic ratios of Mn/Ti are 0.14 and 0.15, much higher than the theoretical value of 0.1, showing that the preparation method of sol-gel and deposition-precipitation would garner a migration of well-dispersed active phase from bulk to surface. A similar phenomenon was also reported in the literature[35]. Particularly, it should be noted that the value of Mn^{4+}/Mn on the surface of MnTi-DP is much higher than that of MnTi-IM and MnTi-SG. This is a promising result that the higher valence manganese state is the original active center for Hg^0 removal.

Table 2 Surface chemical compositions of the samples calculated from the XPS data

Sample	Surface atomic concentrations /%				Surface atomic ratio		
	Mn	Ti	O_α	O_β	Mn/Ti	Mn^{4+}/Mn	$O_\beta/(O_\alpha+O_\beta)$
MnTi-IM	2.51	28.31	55.34	13.84	0.09	0.25	0.20
MnTi-SG	4.18	29.81	47.07	18.94	0.14	0.28	0.28
MnTi-DP	4.24	27.77	49.51	18.51	0.15	0.34	0.27

The XPS patterns of O 1*s* are given in Figure 8(c). According to the literature[32], two types of surface oxygen could be observed in the samples. The peak at about 529.7 eV is assigned to lattice oxygen (noted as O_α), whereas another one at around 531.3 eV is attributed to chemisorbed oxygen (noted

as O_β), such as O_2^{2-} or O^- from oxide defects or hydroxyl-like groups. As shown in Table 2, The $O_\beta/(O_\alpha+O_\beta)$ ratios of MnTi-SG and MnTi-DP are higher than that of MnTi-IM, indicating the presence of abundant chemisorbed oxygen. The surface chemisorbed oxygen O_β might be one of the active sites for Hg^0 removal because of its flexible mobility.

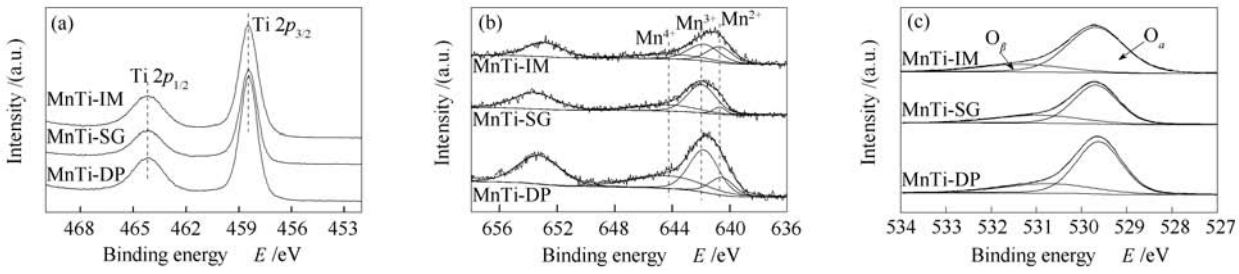

Figure 8　XPS spectra of Mn 2*p* (a), Ti 2*p* (b), and O 1*s* (c) for the samples

3 Conclusions

Compared with MnTi-IM, no clear peak associated with MnO_x appeared in MnTi-SG and MnTi-DP, implying higher dispersion of MnO_x species. Among the three adsorbents, MnTi-DP showed lower reducing temperature, illustrating an increase of reducibility. The Raman intensity of MnTi-DP was lower than that of MnTi-IM, verifying that the presence of MnO_x onto TiO_2 was of amorphous structure. The preparation method of deposition-precipitation and sol-gel would garner a migration of well-dispersed active phase from bulk to surface, resulting in higher ratio of Mn^{4+}/Mn and the presence of abundant chemisorbed oxygen.

The Hg^0 adsorption performance was in the sequence of MnTi-DP > MnTi-SG > MnTi-IM, indicating that the preparation method played a significant role in Hg^0 removal. MnTi-DP had the best SO_2 resistance performance, which may be due to its high dispersion of MnO_2 onto TiO_2 and good redox ability.

References

[1] XU W Q, WANG H R, ZHU T Y, KUANG J Y, JING P F. Mercury removal from coal combustion flue gas by modified fly ash[J]. J Environ Sci, 2013, **25**(2): 393-398.

[2] UDDIN M A, YAMADA T, OCHIAI R. Role of SO_2 for elemental mercury removal from coal combustion flue gas by activated carbon[J]. Energy Fuels, 2008, **22**(4): 2284-2289.

[3] GRANITE E J, PENNLINE H W, HARGIS R A. Novel sorbents for mercury removal from flue gas[J]. Ind Eng Chem Res, 2000, **39**(4): 1020-1029.

[4] STREETS D G, HAO J M, WU Y, JIANG J K, CHAN M, TIAN H Z, FENG X B. Anthropogenic mercury emissions in china[J]. Atmos Environ, 2005, **39**(40): 7789-7806.

[5] YANG S J, GUO Y F, YAN N Q, WU D Q, HE, H P, XIE J K, QU Z, JIA J P. Remarkable effect of the incorporation of titanium on the catalytic activity and SO_2 poisoning resistance of magnetic Mn-Fe spinel for elemental mercury capture[J]. Appl Catal B: Environ, 2011, **101**(3/4): 698-708.

[6] PRESTO A A, GRANITE E J. Survey of catalysts for oxidation of mercury in flue gas[J]. Environ Sci Technol, 2006, **40**(18): 5601-5609.

[7] ZHANG H W, CHEN J T, LIANG P, WANG L. Mercury oxidation and adsorption characteristics of potassium permanganate modified lignite semi-coke[J]. J Environ Sci, 2012, **24**(12): 2083-2090.

[8] MA Y P, XU H M, ZAN Q, YAN N Q, WANG W H. Absorption characteristics of elemental mercury in mercury chloride solutions[J]. J Environ Sci, 2014, **26**(11): 2257-2265.

[9] WU Z B, JIN R B, WANG H Q, LIU Y. Effect of ceria doping on SO_2 resistance of Mn/TiO_2 for selective catalytic reduction of NO with NH_3 at low temperature[J]. Catal Commun, 2009, **10**(6): 935-939.

[10] LIU F D, HE H, DING Y, ZHANG C B. Effect of manganese substitution on the structure and activity of iron titanate catalyst for the selective catalytic reduction of NO with NH_3[J]. Appl Catal B: Environ, 2009, **93**(1/2): 194-204.

[11] 王燕彩, 刘昕, 宁平, 张秋林, 张金辉, 徐利斯, 唐小苏, 王明智. 制备方法对氧化锰八面体分子筛的 NH_3 选择性催化还原 NO_x 性能的影响[J]. 燃料化学学报, 2014, **42**(11): 1357-1364.
(WANG Yan-cai, LIU Xin, NING Ping, ZHANG Qiu-lin, ZHANG Jin-hui, XU Li-si, TANG Xiao-su, WANG Ming-zhi. Effect of preparation methods on selective catalytic reduction of NO_x with NH_3 over manganese oxide octahedral molecular sieves[J]. J Fuel Chem Technol, 2014, **42**(11): 1357-1364.)

[12] SHEN B X, LIU T, ZHAO N, YANG X Y, DENG L D. Iron-doped Mn-Ce/TiO_2 catalyst for low temperature selective catalytic reduction of NO with NH_3[J]. J Environ Sci, 2010, **22**(9): 1447-1454.

[13] JIANG B Q, LIU Y, WU Z B. Low-temperature selective catalytic reduction of NO on MnO_x/TiO_2 prepared by different methods[J]. J Hazard Mater, 2009, **162**(2/3): 1249-1254.

[14] 张信莉, 王栋, 彭建升, 路春美, 徐丽婷. 煅烧温度对 Mn 改性 γ-Fe_2O_3 催化剂结构及低温 SCR 脱硝活性的影响[J]. 燃料化学学报, 2015, **43**(2): 243-250.
(ZHANG Xin-li, WANG Dong, PENG Jian-sheng, LU Chun-mei, XU Li-ting. Influence of calcination temperature on structural property of Mn doped γ-Fe_2O_3 catalysts and low-temperature SCR activity [J]. J Fuel Chem Technol, 2015, **43**(2): 243-250.)

[15] WU Z B, TANG N, XIAO L, LIU Y, WANG H Q. MnO_x/TiO_2 composite nanoxides synthesized by deposition-precipitation method as a

superior catalyst for NO oxidation[J]. J Colloid Interf Sci, 2010, **352**(1): 143-148.
[16] QIAO S H, CHEN J, LI J F, QU Z, LIU P, YAN N Q, JIA J P. Adsorption and catalytic oxidation of gaseous elemental mercury in flue gas over MnO_x/alumina[J]. Ind Eng Chem Res, 2009, **48**(7): 3317-3322.
[17] JI L, SREEKANTH P M, SMIRNIOTIS P G, THIEL S W, PINTO N G. Manganese oxide/titania materials for removal of NO_x and elemental mercury from flue gas[J]. Energy Fuels, 2008, **22**(4): 2299-2306.
[18] XU Y L, ZHONG Q, LIU X Y. Elemental mercury oxidation and adsorption on magnesite powder modified by Mn at low temperature[J]. J Hazard Mater, 2015, **283**: 252-259.
[19] 游淑琳, 周劲松, 侯文慧, 孟帅琦, 高翔, 骆仲泱. 锰改性活性焦脱除合成气中单质汞的影响因素[J]. 燃料化学学报, 2014, **42**(11): 1324-1331.
(YOU Shu-lin, ZHOU Jin-song, HOU Wen-hui, MENG Shuai-qi, GAO Xiang, LUO Zhong-yang. Factors influencing the removal of elemental mercury by Mn-AC sorbent in syngas[J]. J Fuel Chem Technol, 2014, **42**(11): 1324-1331.)
[20] LI H L, WU C Y, LI Y, LI L, ZHAO Y C, ZHANG J Y. Role of flue gas components in mercury oxidation over TiO_2 supported MnO_x-CeO_2 mixed-oxide at low temperature[J]. J Hazard Mater, 2012, **243**: 117-123.
[21] ZHANG A C, ZHENG W W, SONG J, HU S, LIU Z C, XIANG J. Cobalt manganese oxides modified titania catalysts for oxidation of elemental mercury at low flue gas temperature[J]. Chem Eng J, 2014, **236**: 29-38.
[22] LI J W, ZHAO P, LIU S T. SnO_x-MnO_x-TiO_2 catalysts with high resistance to chlorine poisoning for low-temperature chlorobenzene oxidation[J]. Appl Catal A: Gen, 2014, **482**: 363-369.
[23] QI G, YANG R T. Performance and kinetics study for low-temperature SCR of NO with NH_3 over MnO_x-CeO_2 catalyst[J]. J Catal, 2003, **217**(2): 434-441.
[24] HUANG H Y, LONG R Q, YANG R T. A highly sulfur resistant Pt-Rh/TiO_2/Al_2O_3 storage catalyst for NO_x reduction under lean-rich cycles[J]. Appl Catal B: Environ, 2001, **33**(2): 127-136.
[25] KIJLSTRA W S, BIERVLIET M, POELS E K, BLIEK A. Deactivation by SO_2 of MnO_x/Al_2O_3 catalysts used for the selective catalytic reduction of NO with NH_3 at low temperatures[J]. Appl Catal B: Environ, 1998, **16**(4): 327-337.
[26] XU J J, AO Y H, FU D G, YUAN C W. Low-temperature preparation of F-doped TiO_2 film and its photocatalytic activity under solar light[J]. Appl Surf Sci, 2008, **254**(10): 3033-3038.
[27] ZHANG A C, ZHANG Z H, CHEN J J, SHENG W, SUN L S, XIANG J. Effect of calcination temperature on the activity and structure of MnO_x/TiO_2 adsorbent for Hg^0 removal[J]. Fuel Process Technol, 2015, **135**: 25-33.
[28] KHAN A, SMIRNIOTIS P G. Relationship between temperature-programmed reduction profile and activity of modified ferrite-based catalysts for WGS reaction[J]. J Mol Catal A: Chem, 2008, **280**(1/2): 43-51.
[29] KAPTEIJN F, SINGOREDJO L, ANDREINI A, MOULIJN J A. Activity and selectivity of pure manganese oxides in the selective catalytic reduction of nitric oxide with ammonia[J]. Appl Catal B: Environ, 1994, **3**(2/3): 173-189.
[30] GAO X, JIANG Y, FU Y C, ZHONG Y, LUO Z Y, CEN K F. Preparation and characterization of CeO_2/TiO_2 catalysts for selective catalytic reduction of NO with NH_3[J]. Catal Commun, 2010, **11**(5): 465-469.
[31] WAN Q, DUAN L, HE K B, LI J H. Removal of gaseous elemental mercury over a CeO_2-WO_3/TiO_2 nanocomposite in simulated coal-fired flue gas[J]. Chem Eng J, 2011, **170**(2/3): 512-517.
[32] KARAMI A, SALEHI V. The influence of chromium substitution on an iron-titanium catalyst used in the selective catalytic reduction of NO[J]. J Catal, 2012, **292**: 32-43.
[33] CHEN Z H, WANG F R, LI H, YANG Q, WANG L F, LI X H. Low-temperature selective catalytic reduction of NO_x with NH_3 over Fe-Mn mixed-oxide catalysts containing $Fe_3Mn_3O_8$ phase[J]. Ind Eng Chem Res, 2012, **51**(1): 202-212.
[34] GAO R H, ZHANG D S, MAITARAD P, SHI L Y, RUNGROTMONGKOL T, LI H R, ZHANG J P, CAO W G. Morphology-dependent properties of MnO_x/ZrO_2-CeO_2 nanostructures for the selective catalytic reduction of NO with NH_3[J]. J Phys Chem C, 2013, **117**(20): 10502-10511.
[35] YU D Q, LIU Y, WU Z B. Low-temperature catalytic oxidation of toluene over mesoporous MnO_x-CeO_2/TiO_2 prepared by sol-gel method[J]. Catal Commun, 2010, **11**(8): 788-791.

制备方法对 MnO_x-TiO_2 吸附剂脱汞及抗硫性能的影响

张安超[1,*], 张志会[1], 石金明[2], 陈国艳[1], 周长松[3], 孙路石[3]
(1. 河南理工大学 机械与动力工程学院, 河南 焦作 454003;
2. 江西省科学院能源研究所, 江西 南昌 330096;
3. 华中科技大学 煤燃烧国家重点实验室, 湖北 武汉 430074)

摘 要: 针对燃煤烟气中单质汞(Hg^0)不溶于水很难去除和锰基吸附剂抗硫能力差的问题,以浸渍法、溶胶-凝胶法和沉积-沉淀法等三种方法制备 MnO_x-TiO_2 为吸附剂,在固定床实验台架上考察了制备方法对 MnO_x-TiO_2 吸附剂 Hg^0 吸附量和抗硫性能的影响;利用 N_2 吸附/脱附、TG-DSC、XRD、TEM、H_2-TPR 和 XPS 等手段对吸附剂进行表征。结果表明,制备方法对 MnO_x-TiO_2 吸附剂的脱汞活性影响颇大;沉积-沉淀法制备的 MnO_x-TiO_2 吸附剂具有较高的 Hg^0 吸附量和抗硫能力。吸附剂的 BET 比表面积高低与其脱汞活性无直接相关性;与浸渍法和溶胶-凝胶法相比,沉积-沉淀法制备的 MnO_x-TiO_2 吸附剂不但可以增强其还原性和 MnO_x 分散度,而且还会显著提高吸附剂表面 Mn^{4+}/Mn 的比率和表面化学吸附态氧含量,进而增强吸附剂的脱汞活性和抗硫性能。

关键词: 制备方法; MnO_x-TiO_2; 脱汞; 抗硫性能
中图分类号: X511 **文献标识码**: A